Journal of CO_2 Utilization 36 (2020) 187–195

Contents lists available at ScienceDirect

Journal of CO_2 Utilization

journal homepage: www.elsevier.com/locate/jcou

Artificial photosynthesis for alcohol and 3-C compound formation using $BiVO_4$-lamelar catalyst

Patricia Gon Corradini[a,*], Juliana Ferreira de Brito[a,*], Maria Valnice Boldrin Zanoni[b], Lucia Helena Mascaro[a,*]

[a] Department of Chemistry, Federal University of São Carlos, Rod. Washington Luiz, Km 235, CEP 13565-905, São Carlos, SP, Brazil
[b] Institute of Chemistry - Araraquara, UNESP, Rua Francisco Degni, 55, Bairro Quitandinha, 14800-900, Araraquara, SP, Brazil

ARTICLE INFO

Keywords:
Reduction of CO_2
Photocatalysis
Semiconductors
Fuel production
$BiVO_4$ lamellar

ABSTRACT

The high levels of atmospheric CO_2 transformed this compound in a preoccupant pollutant. However, a wide range of semiconductors, including bismuth vanadate ($BiVO_4$), can be applied for CO_2 reduction aiming generation of fuels. This work reports the optimization of the $BiVO_4$ layer synthesis by microwave system using factorial experimental design, where the variables time (5 to 15 min) and temperature (120 to 160 °C) were studied. For evaluation purposes, the materials synthetized were applied in photocatalytic reduction of CO_2. All the $BiVO_4$ materials analyzed promoted the formation of methanol. The best condition was obtained under the material synthesized at 160 °C with 15 min of reaction, where 1.5 mmol L^{-1} $g_{cat}{}^{-1}$ of methanol was produced after 120 min of photocatalysis. For the first time, acetone formation was observed in this kind of material. The best condition for acetone production was acquire with the material prepared at 140 °C with 10 min of synthesis, where 0.030 mmol L^{-1} $g_{cat}{}^{-1}$ was generated after 240 min of CO_2 reduction. Differences in methanol concentration obtained among the samples were probably related to crystallographic patterns of the material, once the presence of Bi_2O_3 or other $BiVO_4$ crystallographic species may affect the efficiency of the material. The results obtained in this work show that the use of $BiVO_4$ layer semiconductor prepared by microwave system for CO_2 reduction leads to the generation of high amounts of methanol under just UV–vis light incidence, aside from promoting the production of acetone.

1. Introduction

There has been an increasingly growing interest in the search of alternatives for the production of renewable energy due to the rapid depletion of fossil fuels coupled with the emission of huge amount of carbon dioxide (CO_2) in the atmosphere during the consumption of fossil fuels [1–3]. Even CO_2 emission in the atmosphere is regarded one of the major causes of global warming, it is also an abundant, cheap, and renewable source of carbon for the production of energy and chemicals [2,4,5]. The production of energy and chemicals from CO_2 can be carried out via reduction process using green techniques [6,7], such as photocatalysis.

Photocatalysis is an environmentally friendly technique based on the use of solar light energy applied in a semiconductor to generate electrons and holes pairs which will undergo reduction and oxidation reaction processes. Solar irradiation provides an infinite source of energy that could be used to supply all the energy needed to sustain and enhance the growth and development of the modern world [8]. In order to produce energy from CO_2 reduction by photocatalysis is necessary a well-designed and robust semiconductor, preferably obtained based on the principles of green chemistry [9]. Usually, photocatalysts are required to be easy to construct, apart from being economically viable, non-toxic and environmentally friendly [10].

A wide range of semiconductors have been investigated and employed in CO_2 reduction since the subject came under the spotlight in the beginning of 2010. During those early years of investigation, the semiconductors that were most widely applied in the area were titanium dioxide modified with copper oxides [11–15]. Recently, there has been a considerable interest in the use of a greater variety of different compositions of semiconductors; in addition, the physical structure of semiconductors has also gained a considerable relevance. Defects in the semiconductor structure, including vacancies, self-interstitials and antisites, often exert influence over doping, minority carrier lifetime and luminescence efficiency [16]. Cezar et al. [17] demonstrated that oxygen defects in V_2O_5 lamellar films can change the magnetic properties of the semiconductor, and aged V_2O_5 films presented higher

* Corresponding authors.
E-mail addresses: patcorradini@gmail.com (P.G. Corradini), jfbrito@ymail.com (J.F. de Brito), lmascaro@ufscar.br (L.H. Mascaro).

https://doi.org/10.1016/j.jcou.2019.10.020
Received 23 August 2019; Received in revised form 17 October 2019; Accepted 26 October 2019
Available online 21 November 2019
2212-9820/

crystallinity and coordination symmetry. Similarly, bismuth vanadate ($BiVO_4$) lamellar semiconductors with vanadium vacancies have been shown to exhibit a relatively higher performance in CO_2 reduction when it comes to methanol formation compared to single-unit-cell $BiVO_4$ layers with poor vanadium vacancies, once it presents new defects levels which increase photoabsorption, quantum efficiency and charge separation [18].

$BiVO_4$ semiconductor is a good example of an environmentally friendly material, once it presents nontoxic and abundant components [19,20]. This semiconductor is known to be widely applied in organic pollutants degradation [21,22], water splitting [23–27] and CO_2 reduction [5,18]. The reason behind the popularity of this semiconductor lies in its properties, which include (i) suitable band gap (around 2.4 eV for monoclinic phase), (ii) good stability in aqueous media, and (iii) low cost [19]. Diverse methods for the preparation of $BiVO_4$ semiconductor have been studied in order to produce this material without having to endure several hours of reflux and aggressive chemicals, seeking a green preparation route [19]. The microwave synthesis technique has proved to be a suitable alternative in this sense due to its operational simplicity, rapid heating, high purity and yield, and good reproducibility [28].

Very few studies published in the literature have reported the use of pure $BiVO_4$ photocatalysts prepared using distinct methodologies for CO_2 reduction via the photocatalysis technique. The use of $BiVO_4$ is based on its conduction and valence bands position, which are suited for water oxidation combined to CO_2 photoreduction [5]. These studies reported the formation of different products, such as methanol in $BiVO_4$ atomic layers [18]; methanol, formaldehyde and formate using polyhedral crystals of monoclinic $BiVO_4$ and hyperbranched crystals of monoclinic $BiVO_4$ catalysts [5], and selective ethanol generation under monoclinic and tetragonal $BiVO_4$ photocatalysts [29]. Precisely, the structure of $BiVO_4$ semiconductor seems to be directly related to the type of products formed from CO_2 reduction.

In the present work, powder lamellar $BiVO_4$ semiconductor was prepared through the application of a fast, simple and environmentally friendly one-step synthesis using microwave and experimental planning. All the materials obtained were applied in CO_2 reduction under aqueous medium using the photocatalysis technique aimed at the production of fuels (such as methanol and acetone) and other compounds with high added value, in a totally renewable way.

2. Experimental section

2.1. Synthesis of $BiVO_4$

Based on the methodology employed by Gao et al. [18] 1.7 mmol of $BiCl_3$ (Sigma-Aldrich®, 98%) and 0.35 g of acetyl bromide (CTAB, Sigma-Aldrich®, 98%) were added to a solution containing 20 ml of ethylene glycol. After vigorous stirring, 2.3 mmol Na_3VO_4 (Sigma-Aldrich®, 90%) were added to the system. However, unlike the mechanism employed in that case, which the system is subjected to conventional heating for 3 h, a microwave system was used (Anton-Paar®) in this present study. By the microwave system, the material was obtained in few minutes. The system was then cooled to room temperature naturally; the final product was collected by centrifuging the mixture with ethanol and water, followed by filtration for 3 times with water. The material was oven dried at 50 °C for 12 h.

An experimental planning was executed with the aim of assessing the influence of temperature, time and stirring speed on the physical and photocatalytic characteristics of the material. The factorial experimental design 2^2 was employed, where the variables time (5–15 min) and temperature (160–240 °C) were evaluated. Two independent materials were prepared at central condition points (10 min; 140 °C) to validate the experimental design. Band gap and methanol production were considered as the responses (dependent variables). The software Chemoface version 1.61 was used to analyze results, with a 90% confidence level of statistical correlation [30].

2.2. Physical characterization

Scanning electron microscopy (SEM) images were obtained with the aid of a field-emission gun scanning electron microscopy (FEG-SEM) Supra 35-VP (Carl Zeiss, Germany). N_2 adsorption measurements were performed at a temperature of -196 °C on a Micromeritics device (ASAP 2420). Prior to analysis, the samples were vacuum treated at 110 °C for 10 h to eliminate physically adsorbed water and gases. Specific surface area was calculated by the Brunauer–Emmett–Teller (BET) equation. Energy-dispersive X-ray spectroscopy (EDX) analyses were used to obtain the atomic ratio between bismuth, vanadium and oxygen, using a Zeiss equipment, model 35. X-ray diffraction (XRD) measurements were performed using Siemens AXS Analytics D5005 X-ray diffractometer (CuK_α = 0.15406 nm, 40 kV and 30 mA), at a scan rate of 1° min^{-1}. Horiba iHR 550 spectrophotometer under green source (544 nm) was used to conduct the Raman spectra analysis. Transmission electron microscopy (TEM) of lamellar $BiVO_4$ were performed by the TECNAI G2F20 microscope. The preparation of samples for TEM consisted of dispersing, with the aid of ultrasound, the catalysts in 2-propanol; deposit them on a carbon-coated copper grid; and subsequently, they were air dried.

2.3. Photocatalytic reduction of CO_2

Photocatalytic experiments for CO_2 photoreduction were performed in a reactor with internal illumination, as shown in Fig. 1. The system was jacketed, allowing a temperature control of 5 °C. Philips 125 W lamp, model HPL-N 1542, without the bulb, protected by a quartz tube, was used for irradiation. In each test, 0.3 g of photocatalyst was suspended in 220 ml of 0.1 mol L^{-1} of $NaHCO_3$ (pH 8.0). The mixture was magnetically stirred in the dark for 30 min prior to irradiation, to allow the system to reach an adsorption / desorption equilibrium. The photocatalytic system was magnetically agitated during the course of illumination. At determined time intervals, 2.0 ml suspensions were collected and analyzed using gas chromatography.

2.4. Products quantification

The quantification of the products methanol, ethanol and acetone was performed by gas chromatography with flame ionization detection (GC-FID - Shimadzu 2010) using Stabilwax column (30 m length, 0.25 mm internal diameter and 25 µm film thickness - Restek, Bellefonte, PA, USA), N_2 as carrier gas at a flow rate of 1.0 ml min^{-1}, injector at 250 °C and detector at 260 °C. The heating ramp started at 40 °C, heated to 46 °C at 2 °C min^{-1} and heated to 170 °C at

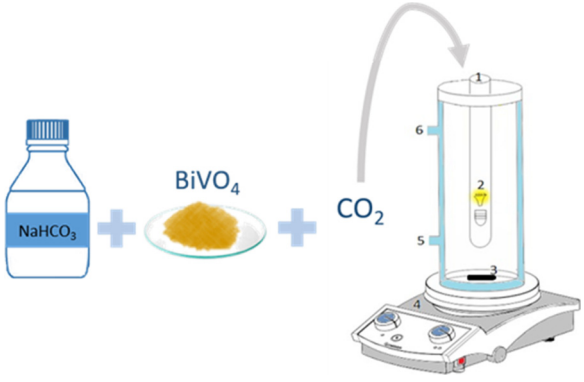

Fig. 1. Representative scheme of the photocatalytic cell composed of 1) quartz tube; 2) lamp (Philips 125 W lamp, model HPL-N 1542, without the bulb); 3) stirring bar; 4) magnetic stirrer and cooling system with entry (5) and exit (6) of water.

45 °C min^{-1}, which was maintained for 3 min. The samples were analyzed by solid phase microextraction technique (SPME) using SPME fiber (CAR/PDMS 75 µm - Supelco). To conduct the solid phase microextraction analysis, the sample with 0.5 ml was transferred to a 1.5 ml sealed container and heated in a bath (Model HB 0.5, IKA) for 7 min at 65 °C. The fiber was exposed to the container headspace for 5 min and then injected into the gas chromatograph [31]. Calibration curves for methanol and ethanol showed linearity in the range of 0.2 µm to 5 mmol L^{-1}, while acetone curves exhibited linearity between 0.02 µm to 0.5 µm. The determination coefficients were 0.96, 0.94 and 0.96 for methanol, ethanol and acetone, respectively.

2.5. Design of experiments for $BiVO_4$ synthesis

Design of experiments (DoE) is an approach which involves the process of planning, designing and analyzing experiments through the use of scientific and statistical principles [32,33]. This method helps to establish the cause-and-effect relationships between the input variables (factors) and the output variables (responses) [33]. The method has a natural green focus; it is centered on how to achieve an efficient design with discrete choice of experiments, low consumption of time and reagents, and under statistically optimal conditions [33–35].

For the purposes of this optimization, 2^2 full factorial design was chosen [36]. Time (5–15 min) and temperature of synthesis (120–160 °C) were evaluated as factors and two levels of each factor were tested. The correlation about the samples and the experimental conditions are presented in Table 1. The syntheses were performed using microwave system, under continuous agitation of 1200 rpm. The sign in parentheses represents the description of the level: negative sign (-) represents the lowest value; positive sign (+) stands for the highest value; and zero (0) is the central condition point. Some parameters, such as band gap and methanol production, were taken as the response and their correlation will be discussed below.

3. Results and discussion

3.1. Physical characterization of $BiVO_4$

The scanning electron microscope (SEM) images of all $BiVO_4$ obtained are shown in Fig. 2. The same flower-like morphology was observed in all the samples. Flower-like hierarchical structures are formed by interlacing nanofoils with thickness of less than 50 nm [37]. Nanofoils have open porous structures; and this can generate large surface area and high incidence of light. Opened porous structures also facilitate the entry of reagents and the release of products. In addition, the use of thin film of nanoparticles leads to a relatively large number of unit cell distortions due to the high surface tension, which can also promote the migration of photogenerated carriers [37]. Nitrogen-adsorption isotherms, shown in Figure S1 in the supplementary information (SI), confirmed that these materials have a significant surface area (30.2 and 26.7 $m^2 g^{-1}$ for sample #4 and #5, respectively), presenting values 10 times higher than that obtained by hydrothermal route [18]. Other catalysts with the same morphology, such as bismuth oxyiodide [38], have shown good efficiency and selectivity for CO_2 reduction.

Table 1
Experimental conditions studied in the factorial planning for $BiVO_4$ semiconductor.

Sample	Temperature / °C	Time / min
#1	(-) 120	(-) 5
#2	(+) 160	(-) 5
#3	(-) 120	(+) 15
#4	(+) 160	(+)15
#5	(0) 140	(0) 10
#6	(0) 140	(0) 10

For hydrothermal routes, the growth mechanism and morphologies of products can be explained based on the dissolution–recrystallization mechanism. As defined under the Gibbs–Thomson law, at lower temperature and higher time, the particles gradually dissolve and recrystallize, leading to crystal growth; at higher temperatures and short times promote smaller and semispherical particles [39]. In the microwave-assisted synthesis, the influence of temperature and time of synthesis on morphology does not appear to be so evident. As the heating is done from the inside out, and the synthesis is conducted at very short intervals of time, it is likely that the mechanism of formation of $BiVO_4$ is not affected under the conditions studied. The lamellar structure obtained can be attributed to the presence of acetyl bromide (CTAB), which promotes the directed growth of $BiVO_4$, as described by Gao et al. [18].

The analysis of the samples purity was performed by EDX technique. For the purposes of illustration, Fig. 3a shows the analysis of purity for sample #2. The same EDX spectrum was obtained in all the cases; the semiconductor was found to be solely composed of oxygen, vanadium and bismuth. These results indicate that the methodology employed to produce the powder led to the generation of a semiconductor free of residual synthesis or other interfering compounds. Table 2 presents the EDX composition for all the obtained materials. Most of the samples exhibited a similar proportion of atomic percentage, with approximately 60% of oxygen and 20% each of bismuth and vanadium elements; this confirms the formation of $BiVO_4$. The only difference was observed in samples #3, #5 and #6, where the atomic percentage of bismuth was found to be higher than that of vanadium.

X-ray diffraction and Raman spectroscopy analysis were carried out aiming to investigate the formation of other compounds. XRD spectra of all the bismuth vanadate materials are shown in Fig. 3b. The crystalline orientation indexed to $BiVO_4$ is orthorhombic (JCPDS No. 85-1730, shown in Fig. 3b). An enlargement of the diffraction peaks is common for the lamellar structures; this shows that the desired structure was obtained for all the syntheses [18]. Samples # 3, # 5 and # 6 showed the formation of bismuth oxide (JCPDS No. 76-2478, shown in Fig. 3b) [40]; this by-product is a semiconductor found to be characterized by good photoconductivity [41,42]. The co-formation of Bi_2O_3 in $BiVO_4$ is reported for other mechanisms of synthesis, such as the hydrothermal method [43] and the precipitation method [44].

Raman spectroscopy technique was used to analyze the metal-oxygen structures and bonds through their vibrational characteristics. Fig. 3c shows the Raman spectra for all the $BiVO_4$ samples. The Raman spectrum for $BiVO_4$ indicates the presence of VO_4^- tetrahedron [45]. The band close to 200 cm^{-1} can be attributed to the rotational/translational external modes of VO_4^{-3} [46]. The asymmetric and symmetric flexion modes of VO_4^{-3} can be observed at 326 cm^{-1} and 364 cm^{-1}, respectively [47]. The band close to 807 cm^{-1} and the weak shoulder close to 700 cm^{-1} refer to the vibrational mode A_g, which is related to the antisymmetric and symmetric stretching modes of long and short V—O bonds, respectively [18,45]. In comparison to the typical frequencies of monoclinic $BiVO_4$, all the vibrations were shifted to lower frequencies, and these differences are correlated to different surface-to-volume ratio of $BiVO_4$, caused by the geometry of the material [48]. With respect to Raman spectroscopy analyses, no signals related to Bi_2O_3 or other species were observed (Bi_2O_3 signals at 115–130 cm^{-1}, 280-320 cm^{-1}, and 445–485 cm^{-1} [49]).

Transmission electron microscopy (TEM) images of sample #4 in different magnitudes are presented in Fig. 4. Fig. 4a presents the top view of $BiVO_4$ powder with lamellar characteristics; similar to those presented in the SEM images of Fig. 2. Fig. 4b shows an approximation where it is possible to identify the size of the material nanoparticles, which are in the order of 7.0 nm. High resolution TEM images can be observed in Figs. 4c and 4d. In Fig. 4c, one can observe the presence of crystal structures evidenced by the crystallographic planes seen along the surface of the material. Fig. 4d confirms the presence of $BiVO_4$ by the lattice spacing measuring 3.1 Å (distance related to plane [112] of

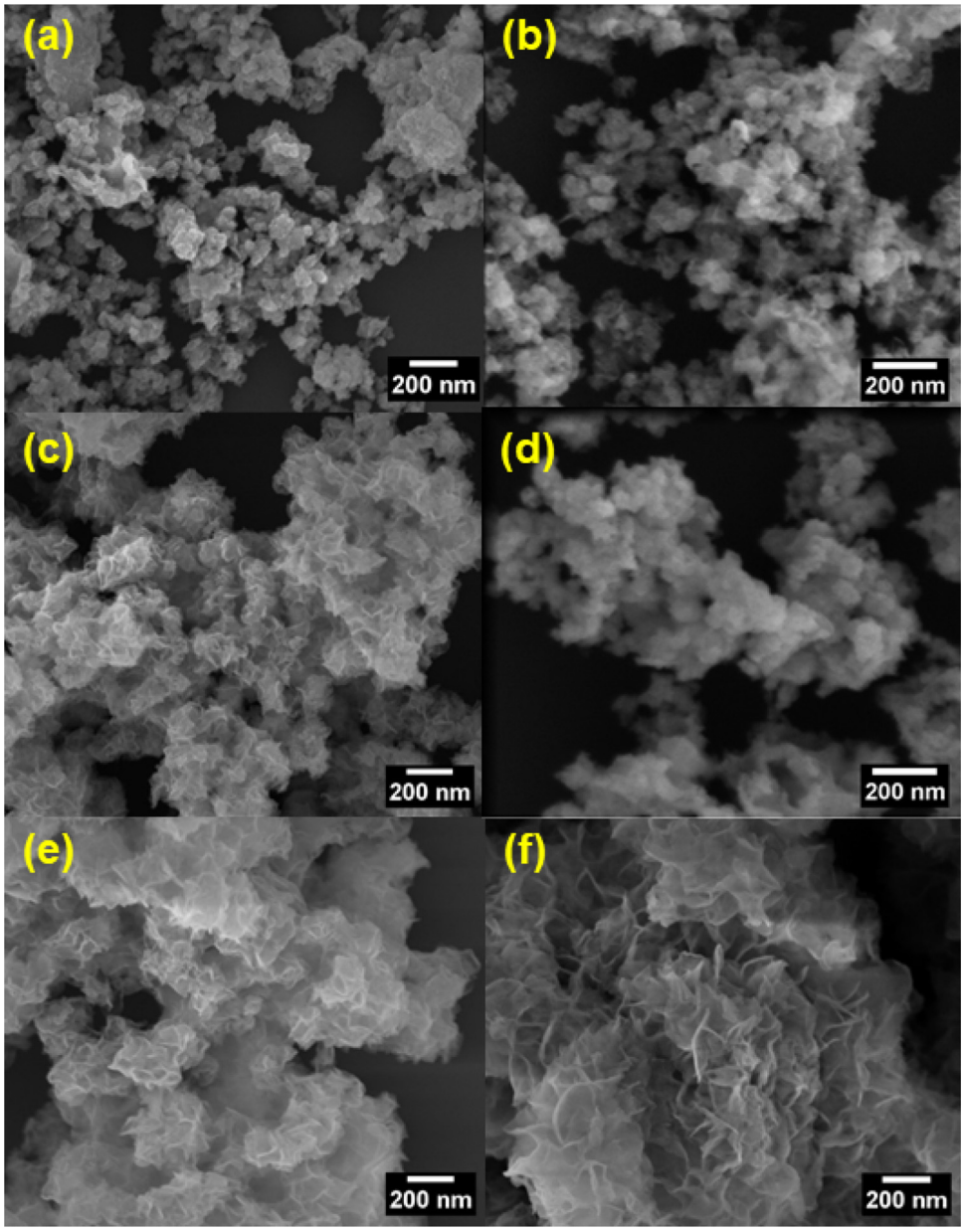

Fig. 2. Morphological images of $BiVO_4$ obtained by microwave synthesis technique at (a) 120 °C for 5 min (sample #1), (b) 160 °C for 5 min (sample #2), (c) 120 °C for 15 min (sample #3), (d) 160 °C for 15 min (sample #4), (e) sample #5 and (f) sample #6, both synthesized at 140 °C for 10 min.

$BiVO_4$), the more intense phase of the semiconductor, which is obtained in the peak at 2θ = 28.8, in agreement with the results presented in the XRD data in Fig. 3b.

Tauc plot for all the materials is presented in Fig. 5. $BiVO_4$ material has a direct permissible electronic transition between the bands. Through the extrapolation of the linear region was possible to estimate the band gap energies (Eg) presented in Table 2. The band gap energy reported for monoclinic $BiVO_4$ is usually between 2.4–2.5 eV [50,51]. Abraham et al. produced $BiVO_4$ nanoparticles using microwave irradiation; the semiconductor exhibited a band gap of 2.73 eV, one of the largest band gaps reported for non-doped material [52]. Gao et al. [18] studied $BiVO_4$ on lamellar form, but this material was obtained by the hydrothermal route, which took 3 h or 12 h of reaction to be accomplished. The authors reported high bang gap value, close to 3.0 eV [18]. For $BiVO_4$ materials obtained in the present study, the band gap values obtained varied between 2.54–3.18 eV; these are higher than those reported in the literature. The higher band gaps were observed for samples #3, #5 and #6; these samples presented the Bi_2O_3 diffraction peaks in Fig. 3b, which may alter the properties of these materials [41,42]. This behavior may indicate the formation of heterojunction between $BiVO_4$ and Bi_2O_3.

Some authors have investigated the use of Bi_2O_3/$BiVO_4$ for bisphenol degradation, and noted a variation in the energy bands of Bi_2O_3 and $BiVO_4$ with the diffusion of charge carriers until an equilibrium is reached between the Fermi levels of Bi_2O_3 and $BiVO_4$ [10]. According to Chen et al. [17] the presence of small quantities of Bi_2O_3 on $BiVO_4$ promotes separation of charges carriers and a better diffusion of these charges to the semiconductor surface.

Pareto graph was constructed in order to analyze the influence of temperature and time on the band gap of the material (Fig. 5b). In this graphical representation, each bar is proportional to the standardized effect (which is the estimated effect divided by its standard error) [53]. The red vertical line is used to determine which effects are statistically significant at 90% confidence level. The factor that surpasses the vertical line corresponds to an effect which is statistically significant in terms of the change of the analyzed response. In the studied range, no

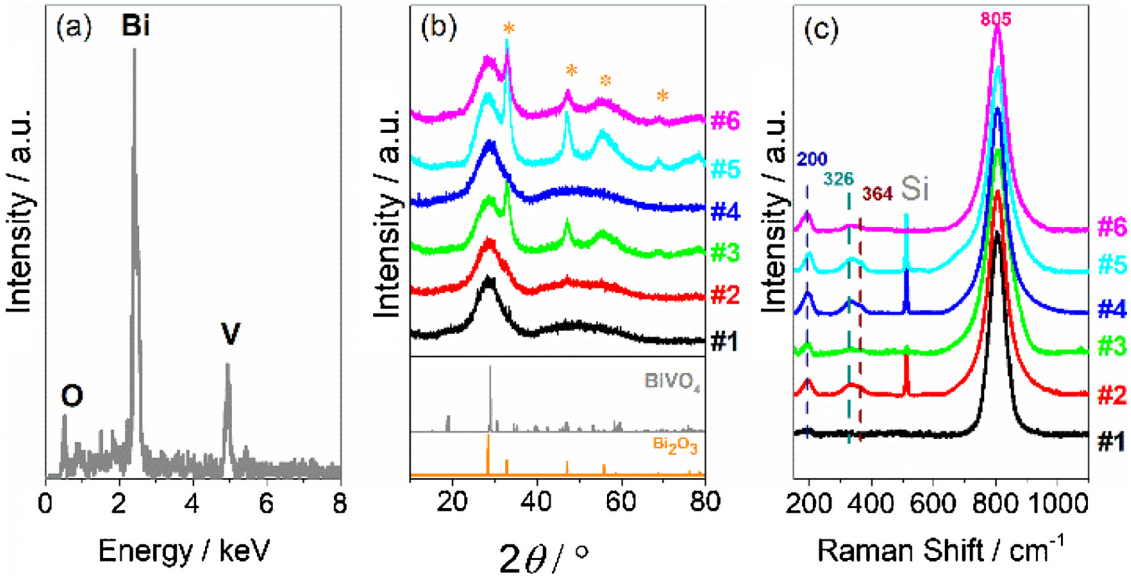

Fig. 3. (a) EDX spectrum of $BiVO_4$ sample #2. (b) XRD patterns and (b) Raman spectra of the samples of all obtained $BiVO_4$ materials prepared using microwave synthesis under the factorial planning conditions.

Table 2
Semi-quantitative atomic percentage of $BiVO_4$ semiconductor samples obtained by EDX analysis and the respective band gap energy calculated from the diffuse reflectance of each material.

Sample	Temperature / °C	Band gap
#1	18 : 21 : 61 (1 : 1.1 : 3.4)	2.92 eV
#2	15 : 17 : 68 (1 : 1.1 : 4.5)	2.77 eV
#3	24 : 16 : 60 (1.5 : 1 : 3.75)	3.18 eV
#4	19 : 22 : 59 (1 : 1.1 : 3)	2.54 eV
#5	20 : 13 : 67 (1.5 : 1 : 5)	2.98 eV
#6	20 : 17 : 63 (1.2 : 1 : 3.7)	3.03 eV

direct correlation was found between the synthesis time factor and the band gap values. On the other hand, an inverse correlation was found between the temperature and the interaction time-temperature, where a rise in temperature was found to lead to a decrease in band gap. Furthermore, the time-temperature interaction was also found to affect the band gap responses. Figure S2, in the SI, shows the correlation between time-temperature of the microwave-assisted synthesis and the band gap of the obtained materials. The changes observed in band gap must be related to the presence of secondary phases, such as Bi_2O_3, which present a relatively higher band gap (~2.7 eV) compared to $BiVO_4$ [10]. The band gap of the material influences in the band alignment, interfering in the products formation from CO_2 reduction, as will be presented later.

3.2. Products obtained from CO_2 reduction

The factorial planning led to the preparation of semiconductors with band gap values ranging from 2.54 to 3.18 eV. As discussed previously, the band gap energy for monoclinic $BiVO_4$ is 2.5 eV; however, a higher range of values have already been reported in the literature [19], due to the use of different synthesis methods. These band gaps are related to semiconductors that can be activated by ultraviolet and visible light incidence. In this sense, CO_2 reduction was performed for all the semiconductors under UV–vis light incidence. The products quantified over the reaction time are presented in Fig. 6.

The selectivity of the products largely depends on the morphology and crystalline structure of $BiVO_4$ catalyst. As in the study on monoclinic $BiVO_4$ obtained by microwave-assisted hydrothermal method, the production of ethanol was detected; however, these structures did not promote a significant production of methanol [29]. Though, the major role of $BiVO_4$ semiconductor is its ability to produce methanol as the main product by CO_2 reduction via photocatalysis technique [5,18]. It is not uncommon to have methanol as the main product of CO_2 reduction, once it presents a relatively smaller thermodynamic potential (E° = -0.38 V) compared to other products such as acetone (E° = -0.61 V), for example [54,55].

No reports are found in the literature regarding the use of $BiVO_4$ as catalyst for the production of acetone. In the present study, acetone was produced under the three synthesis conditions. The samples prepared under 5 min of microwave or at 120 °C were not able to produce quantifiable quantities of acetone from CO_2 reduction. However, the samples prepared under higher periods of time and temperatures and which contained bismuth oxide in their composition (according to XRD of Fig. 3b) presented a higher acetone formation. Using sample #6, 30.0 μmol g_{cat}^{-1} of acetone were generated after 240 min of photocatalysis. These results show that the presence of Bi_2O_3 in the semiconductor composition, which generates $BiVO_4$-Bi_2O_3 junction, leads to homolytic cleavage of methanol, contributing to the formation of acetone.

Acetone is a complex compound to be formed from CO_2 reduction largely due to the 3C present in its structure. Just a few researchers had reported formation of acetone using photocatalytic CO_2 reduction [56,57]. However, according to the best of our knowledge, that is the first time that acetone is quantified using $BiVO_4$ as catalyst for photocatalytic CO_2 reduction. In essence, this is the a very important contribution of the present work to the literature.

The formation of acetone probably occurs from the reaction of products with 1C, such as methanol, formed initially in the system, with intermediates present in solution, such as $OH^{\cdot}$, H^+ and $CH_3^{\cdot}$ [58,59]. Probably because of that, the production of acetone reaches a high concentration at a period of time different from that of the production of methanol under sample #4, even without the Bi_2O_3 in this particular sample. The possible reaction pathway that lead to the formation of methanol and acetone is presented in Eq.s 1 to 4.

$$CO_2 + 1e^- \rightarrow CO_2^{\cdot -} \quad (1)$$

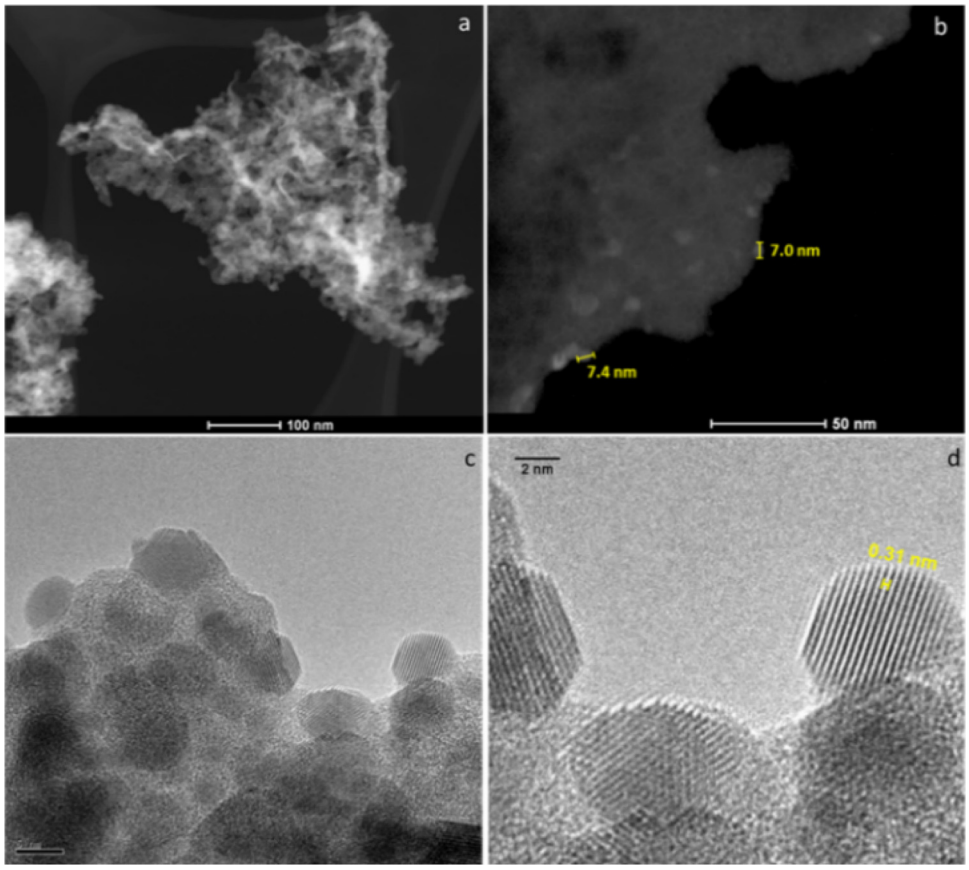

Fig. 4. TEM images with different magnitudes of $BiVO_4$ sample #4.

$$CO_2^{\bullet -} + 5e^- + 6H^+ \rightarrow CH_3OH + H_2O \quad (2)$$

$$CH_3OH \rightarrow CH_3^{\bullet} + OH^{\bullet} \quad (3)$$

$$CO_2^{\bullet -} + 2CH_3^{\bullet} + 1e^- + 2H^+ \rightarrow CH_3COCH_3 + H_2O \quad (4)$$

Under sample #4, a high concentration of methanol was generated up to 120 min of reaction, after this time onwards, a decrease was observed in methanol production. This reduction can be correlated to the acetone formation as by-product of CO_2 reduction. Another possibility can be relate to a deactivation of the material during the time of reaction, as reported previously by Sommers and coworkers [5]. According to them, during CO_2 reduction, $BiVO_4$ becomes engraved by Bi_2O_{4-x} nanoparticles, which block the active surface. As sample #4 was the most active semiconductor, it probably reaches deactivation faster than the other semiconductors investigated.

In order to develop a possible mechanism for CO_2 reduction using $BiVO_4$ semiconductor, the potentials of the valence band (VB) and the conduction band (CB) of the material were estimated based on the work of Gao et al. [18]. In their work the authors obtained a lamellar $BiVO_4$ semiconductor with mean valence band energy of 2.42 eV which was estimated by XPS analysis [18]. This value is smoothly distinct from the

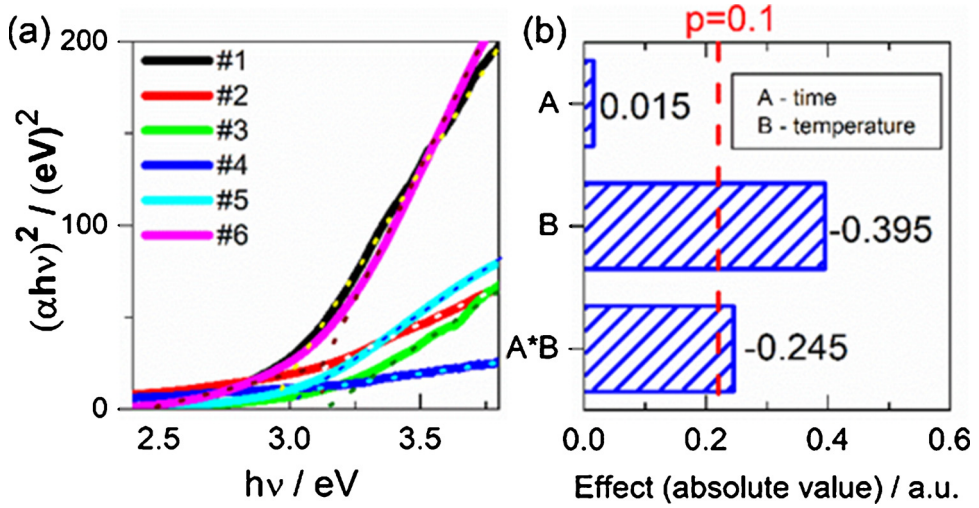

Fig. 5. (a) Diffuse reflectance data $(\alpha h\nu)^2$ *vs.* photon energy for $BiVO_4$ powder semiconductor prepared under the factorial planning conditions. (b) Pareto graph for band gap response.

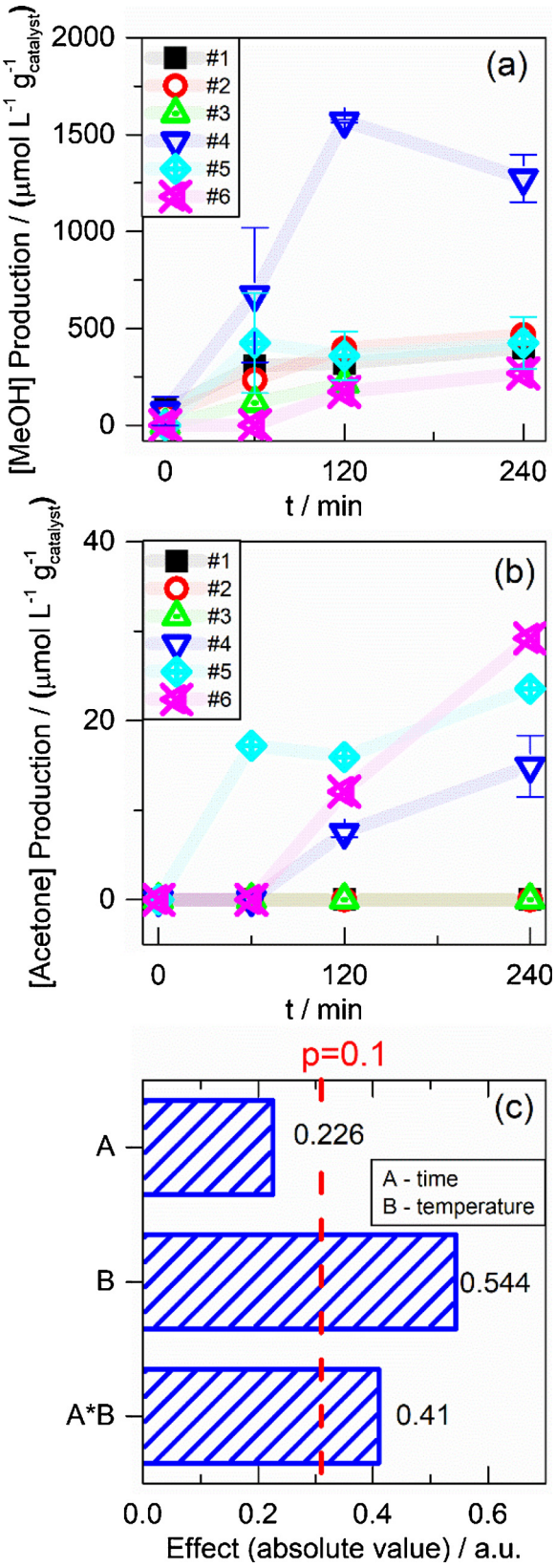

Fig. 6. Concentration of (a) methanol and (b) acetone derived from CO_2 reduction during the time of reaction under 0.1 mol L^{-1} $NaHCO_3$ pH 8 supporting electrolyte and UV–vis light for all $BiVO_4$ semiconductors prepared based on factorial planning. (c) Pareto graph for methanol production responses.

value obtained by the Mulliken electronegativity theory based on Eq. 5 [20,60]:

$$E_{VB} = X - E^e + 0.5E_{bg} \quad (5)$$

where E_{VB} is the potential of the VB; X is the semiconductor electronegativity, which is calculated by the geometric mean values of the atoms of the molecule (6.04 eV in the case of monoclinic $BiVO_4$); E^e is the energy of free electrons on the hydrogen scale (4.5 eV); and E_{bg} is the potential of the band gap (the mean value considered in this case was 2.90 eV). The difference in VB values can be attributed to the influence of the lamellar structure of the material. The potential of the CB was calculated based on the potential of the VB and the E_{bg}, according to Eq. 6.

$$E_{CB} = E_{VB} - E_{bg} \quad (6)$$

The VB and CB values obtained for the mean value of the materials prepared in this work were 2.42 eV and -0.48 eV, respectively. It is worth noting that the band alignment of the lamellar $BiVO_4$ semiconductor led to a more selective methanol formation. This result differs from that of the studies published in the literature, which show ethanol formation under photocatalytic CO_2 reduction using this same semiconductor [29]. Additionally, the formation of acetone probably occurs via radical reactions beginning from methanol production. Thus, a mechanism involving charge transfer and products formation was constructed based on both the results obtained in this work and those reported in the literature [61–63]. The mechanism is presented in Fig. 7.

To find out whether time and temperature of synthesis affected the production of methanol, the Pareto graph in Fig. 6c was presented for the concentrations obtained in 2 h of CO_2 photoreduction. With regard to the band gap, the temperature and time-temperature interaction were found to be positively related to the amount of methanol produced. In this sense, an increase in these factors resulted in an increase in methanol production. Concerning the different synthesis conditions investigated, the optimal synthesis conditions were found to be at the temperature of 160 °C and reaction time of 15 min; these conditions are consistent with the information presented in Fig. 5b. These results are in agreement with the findings of the work published by Gao et al. [18] who concluded that higher temperature promotes vanadium vacancies, and this in turn leads to better materials for CO_2 reductions.

4. Conclusions

The application of the factorial experimental design contributed to the improvement of the methodology of $BiVO_4$ synthesis. The preparation of the semiconductors was performed by clean, green, and easy microwave method. All the prepared samples led to the production of methanol by CO_2 photoreduction under just UV–vis light incidence with at least 60 min of reaction. The sample prepared under 160 °C with 15 min of synthesis presented a significant activity in terms of methanol formation, reaching 1.50 mmol L^{-1} g_{cat}^{-1} after 120 min of reaction. Acetone formation was also identified in the reaction conducted with catalysts prepared at 160 °C and 140 °C for 15 and 10 min, respectively. For $BiVO_4$ sample prepared under 140 °C for 10 min, 30.0 µmol g_{cat}^{-1} of acetone were obtained. The results accomplished in this work point to a significant improvement when compared with those reported in the literature, particularly in terms of the high concentration of methanol produced and the amount of acetone formed through the sole application of the photocatalysis technique.

Declaration of Competing Interest

The authors declare that they have no known competing financial interests or personal relationships that could have appeared to influence the work reported in this paper.

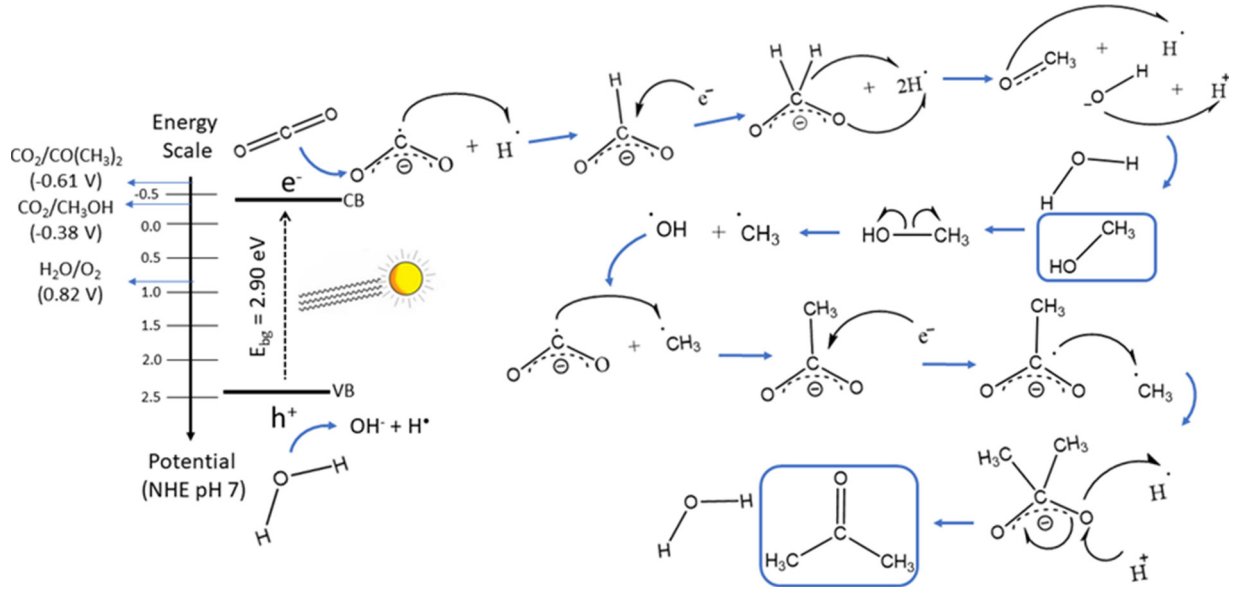

Fig. 7. Mechanism of charge transfer and products formation of $BiVO_4$ semiconductor using photocatalysis technique with UV–vis light irradiation.

Acknowledgments

The authors thank the Domingos Sérgio and Prof. Ernesto Urquieta, of Centro de Pesquisa em Materiais Avançados e Energia (CPqMAE), for N_2 adsorption measurements and the Laboratory of Structural Characterization (LCE/DEMa/UFSCar) for the general facilities. The authors are grateful to the following Brazilian research funding agencies for the financial support provided during the course of this research: Coordenação de Aperfeiçoamento de Pessoal de Nível Superior - Brasil (CAPES) - Finance Code 001; Conselho Nacional de Pesquisa e Desenvolvimento (CNPq); and São Paulo Research Foundation (FAPESP), grant #2018/16401-8, #2018/02950-0, #2013/07296-2, #2014/50249-8).

Appendix A. Supplementary data

Supplementary material related to this article can be found, in the online version, at doi:https://doi.org/10.1016/j.jcou.2019.10.020.

References

[1] Y. Yang, H. Zhong, R.T. He, X.G. Wang, J. Cheng, G.D. Yao, F.M. Jin, Synergetic conversion of microalgae and CO2 into value-added chemicals under hydrothermal conditions, Green Chem. 21 (2019) 1247–1252, https://doi.org/10.1039/c8gc03645d.

[2] Y. Ahn, J. Byun, D. Kim, B.-S. Kim, C.-S. Lee, J. Han, System-level analysis and life cycle assessment of CO2 and fossil-based formic acid strategies, Green Chem. (2019), https://doi.org/10.1039/C9GC01280J.

[3] D.-H. Lan, Y.-X. Gong, N.-Y. Tan, S.-S. Wu, J. Shen, K.-C. Yao, B. Yi, C.-T. Au, S.-F. Yin, Multi-functionalization of GO with multi-cationic ILs as high efficient metal-free catalyst for CO2 cycloaddition under mild conditions, Carbon 127 (2018) 245–254, https://doi.org/10.1016/j.carbon.2017.11.007.

[4] Y. Chen, T. Mu, Conversion of CO2 to value-added products mediated by ionic liquids, Green Chem. (2019), https://doi.org/10.1039/C9GC00827F.

[5] J.M. Sommers, N.P. Alderman, C.J. Viasus, S. Gambarotta, Revisiting the behaviour of $BiVO_4$ as a carbon dioxide reduction photo-catalyst, Dalton Trans. 46 (2017) 6404–6408, https://doi.org/10.1039/C7DT00414A.

[6] D.-H. Lan, F.-M. Yang, S.-L. Luo, C.-T. Au, S.-F. Yin, Water-tolerant graphene oxide as a high-efficiency catalyst for the synthesis of propylene carbonate from propylene oxide and carbon dioxide, Carbon 73 (2014) 351–360, https://doi.org/10.1016/j.carbon.2014.02.075.

[7] D.-H. Lan, H.-T. Wang, L. Chen, C.-T. Au, S.-F. Yin, Phosphorous-modified bulk graphitic carbon nitride: facile preparation and application as an acid-base bifunctional and efficient catalyst for CO2 cycloaddition with epoxides, Carbon 100 (2016) 81–89, https://doi.org/10.1016/j.carbon.2015.12.098.

[8] S.N. Habisreutinger, L. Schmidt-Mende, J.K. Stolarczyk, Photocatalytic reduction of CO2 on TiO2 and other semiconductors, Angew. Chemie Int. Ed. English 52 (2013) 7372–7408, https://doi.org/10.1002/anie.201207199.

[9] F. Iacopi, M. McIntosh, Opportunities and perspectives for green chemistry in semiconductor technologies, Green Chem. (2019), https://doi.org/10.1039/C9GC01058K.

[10] P. Qiu, B. Park, J. Choi, M. Cui, J. Kim, J. Khim, BiVO4/Bi2O3 heterojunction deposited on graphene for an enhanced visible-light photocatalytic activity, J. Alloys. Compd. 706 (2017) 7–15, https://doi.org/10.1016/j.jallcom.2017.02.232.

[11] S. Qin, F. Xin, Y. Liu, X. Yin, W. Ma, Photocatalytic reduction of CO2 in methanol to methyl formate over CuO–TiO2 composite catalysts, J. Colloid Interface Sci. 356 (2011) 257–261, https://doi.org/10.1016/j.jcis.2010.12.034.

[12] H.W. Slamet, E. Nasution, K. Purnama, J.G. Riyani, Effect of copper species in a photocatalytic synthesis of methanol from Carbon Dioxide over copper-doped titania catalysts, World Appl. Sci. J. 6 (2009) 112–122.

[13] H.W. Slamet, E. Nasution, S. Purnama, J.G. Kosela, Photocatalytic reduction of CO2 on copper-doped Titania catalysts prepared by improved-impregnation method, Catal. Commun. 6 (2005) 313–319, https://doi.org/10.1016/j.catcom.2005.01.011.

[14] N. Singhal, A. Ali, A. Vorontsov, C. Pendem, U. Kumar, Efficient approach for simultaneous CO and H-2 production via photoreduction of CO2 with water over copper nanoparticles loaded TiO2, Appl Catal a-Gen 523 (2016) 107–117, https://doi.org/10.1016/j.apcata.2016.05.027.

[15] C. Li, Y. Xu, W. Tu, G. Chen, R. Xu, Metal-free photocatalysts for various applications in energy conversion and environmental purification, Green Chem. 19 (2017) 882–899, https://doi.org/10.1039/C6GC02856J.

[16] A. Janotti, C.G. Van de Walle, Native point defects in ZnO, Phys. Rev. B 76 (2007), https://doi.org/10.1103/PhysRevB.76.165202.

[17] A.B. Cezar, I.L. Graff, J. Varalda, W.H. Schreiner, D.H. Mosca, Oxygen-vacancy-induced room-temperature magnetization in lamellar V2O5 thin films, J. Appl. Phys. 116 (2014) 163904, , https://doi.org/10.1063/1.4899249.

[18] S. Gao, B. Gu, X. Jiao, Y. Sun, X. Zu, F. Yang, W. Zhu, C. Wang, Z. Feng, B. Ye, Y. Xie, Highly efficient and exceptionally durable CO_2 photoreduction to methanol over freestanding defective single-unit-Cell bismuth vanadate layers, J. Am. Chem. Soc. 139 (2017) 3438–3445, https://doi.org/10.1021/jacs.6b11263.

[19] L.H. Mascaro, A. Pockett, J.M. Mitchels, L.M. Peter, P.J. Cameron, V. Celorrio, D.J. Fermin, J.S. Sagu, K.G.U. Wijayantha, G. Kociok-Köhn, F. Marken, One-step preparation of the BiVO4 film photoelectrode, J. Solid State Electrochem. 19 (2014) 31–35, https://doi.org/10.1007/s10008-014-2495-y.

[20] L. Chen, Q. Zhang, R. Huang, S.-F. Yin, S.-L. Luo, C.-T. Au, Porous peanut-like Bi2O3–BiVO4 composites with heterojunctions: one-step synthesis and their photocatalytic properties, J. Chem. Soc. Dalton Trans. 41 (2012) 9513–9518, https://doi.org/10.1039/C2DT30543G.

[21] W. Shi, Y. Yan, X. Yan, Microwave-assisted synthesis of nano-scale BiVO4 photocatalysts and their excellent visible-light-driven photocatalytic activity for the degradation of ciprofloxacin, Chem. Eng. J. 215–216 (2013) 740–746, https://doi.org/10.1016/j.cej.2012.10.071.

[22] M.R. da Silva, L.H. Dall'Antonia, L.V.A. Scalvi, D.I. dos Santos, L.O. Ruggiero, A. Urbano, Deposition and characterization of BiVO4 thin films and evaluation as photoanodes for methylene blue degradation, J. Solid State Electrochem. 16 (2012) 3267–3274, https://doi.org/10.1007/s10008-012-1765-9.

[23] C. Ding, J. Shi, D. Wang, Z. Wang, N. Wang, G. Liu, F. Xiong, C. Li, Visible light driven overall water splitting using cocatalyst/BiVO4 photoanode with minimized bias, J. Chem. Soc. Faraday Trans. 15 (2013) 4589–4595, https://doi.org/10.1039/C3CP50295C.

[24] R. Saito, Y. Miseki, K. Sayama, Photoanode characteristics of multi-layer composite BiVO4 thin film in a concentrated carbonate electrolyte solution for water splitting, J. Photochem. Photobiol. A: Chem. 258 (2013) 51–60, https://doi.org/10.1016/j.

jphotochem.2013.02.019.
[25] S.K. Pilli, T.G. Deutsch, T.E. Furtak, L.D. Brown, J.A. Turner, A.M. Herring, BiVO4/CuWO4 heterojunction photoanodes for efficient solar driven water oxidation, J. Chem. Soc. Faraday Trans. 15 (2013) 3273–3278, https://doi.org/10.1039/C2CP44577H.
[26] H.W. Jeong, T.H. Jeon, J.S. Jang, W. Choi, H. Park, Strategic modification of BiVO4 for improving photoelectrochemical water oxidation performance, J. Phys. Chem. C 117 (2013) 9104–9112, https://doi.org/10.1021/jp400415m.
[27] S. Hernández, C. Ottone, S. Proto, K. Tolod, M. Díaz de los Bernardos, A. Solé-Daura, J.J. Carbó, C. Godard, S. Castillón, N. Russo, G. Saracco, C. Claver, Core-substituted naphthalenediimides anchored on BiVO4 for visible light-driven water splitting, Green Chem. 19 (2017) 2448–2462, https://doi.org/10.1039/C7GC00125H.
[28] X. Chen, L. Li, T. Yi, W. Zhang, X. Zhang, L. Wang, Microwave assisted synthesis of sheet-like Cu/$BiVO_4$ and its activities of various photocatalytic conditions, J. Solid State Chem. 229 (2015) 141–149, https://doi.org/10.1016/j.jssc.2015.05.026.
[29] Y. Liu, B. Huang, Y. Dai, X. Zhang, X. Qin, M. Jiang, M.-H. Whangbo, Selective ethanol formation from photocatalytic reduction of carbon dioxide in water with BiVO4 photocatalyst, Catal. Commun. 11 (2009) 210–213, https://doi.org/10.1016/j.catcom.2009.10.010.
[30] C.A. Nunes, V.O. Alvarenga, A. de Souza Sant'Ana, J.S. Santos, D. Granato, The use of statistical software in food science and technology: advantages, limitations and misuses, Food Res. Int. 75 (2015) 270–280, https://doi.org/10.1016/j.foodres.2015.06.011.
[31] J.F. Brito, J.A.L. Perini, S. Perathoner, M.V.B. Zanoni, Turning carbon dioxide into fuel concomitantly to the photoanode-driven process of organic pollutant degradation by photoelectrocatalysis, Electrochim. Acta 306 (2019) 277–284, https://doi.org/10.1016/j.electacta.2019.03.134.
[32] J. Antony, 2 - fundamentals of design of experiments, in: J. Antony (Ed.), Design of Experiments for Engineers and Scientists, Butterworth-Heinemann, Oxford, 2003, pp. 6–16.
[33] S. Beg, S. Swain, M. Rahman, M.S. Hasnain, S.S. Imam, Chapter 3 - application of design of experiments (DoE) in pharmaceutical product and process optimization, in: S. Beg, M.S. Hasnain (Eds.), Pharmaceutical Quality by Design, Academic Press, 2019, pp. 43–64.
[34] R.A. Daziano, B. Farooq, Workshop Synthesis: new directions in experimental design, Transp. Res. Procedia 32 (2018) 448–453, https://doi.org/10.1016/j.trpro.2018.10.052.
[35] S.S. Garud, I.A. Karimi, M. Kraft, Design of computer experiments: a review, Comput. Chem. Eng. 106 (2017) 71–95, https://doi.org/10.1016/j.compchemeng.2017.05.010.
[36] J. Antony, 6 - full factorial designs, in: J. Antony (Ed.), Design of Experiments for Engineers and Scientists, Butterworth-Heinemann, Oxford, 2003, pp. 54–72.
[37] J.Q. Li, M.M. Cui, Z.Y. Guo, Z.X. Liu, Z.F. Zhu, Synthesis of dumbbell-like CuO-BiVO4 heterogeneous nanostructures with enhanced visible-light photocatalytic activity, Mater. Lett. 130 (2014) 36–39, https://doi.org/10.1016/j.matlet.2014.05.084.
[38] N. Han, Y. Wang, H. Yang, J. Deng, J.H. Wu, Y.F. Li, Y.G. Li, Ultrathin bismuth nanosheets from in situ topotactic transformation for selective electrocatalytic CO2 reduction to formate, Nat. Commun. 9 (2018), https://doi.org/10.1038/s41467-018-03712-z.
[39] U.M. Garcia-Perez, A. Martinez-de la Cruz, S. Sepulveda-Guzman, J. Peral, Low-temperature synthesis of BiVO4 powders by Pluronic-assisted hydrothermal method: effect of the surfactant and temperature on the morphology and structural control, Ceram. Int. 40 (2014) 4631–4638, https://doi.org/10.1016/j.ceramint.2013.09.002.
[40] I.N. Reddy, C.V. Reddy, A. Sreedhar, M. Cho, D. Kim, J. Shim, Systematic studies of Bi2O3 hierarchical nanostructural and plasmonic effect on photoelectrochemical activity under visible light irradiation, Ceram. Int. (2019), https://doi.org/10.1016/j.ceramint.2019.05.214.
[41] E. Luévano-Hipólito, L.M. Torres-Martínez, C. Triana, S.W. Lee, Ink-jet Bi2O3 films and powders for CO2 capture and self-cleaning applications, Thin Solid Films 677 (2019) 83–89, https://doi.org/10.1016/j.tsf.2019.03.020.
[42] H. Lim, S.B. Rawal, Integrated Bi2O3 nanostructure modified with Au nanoparticles for enhanced photocatalytic activity under visible light irradiation, Prog. Nat. Sci. 27 (2017) 289–296, https://doi.org/10.1016/j.pnsc.2017.04.003.
[43] L. Chen, J. Wang, D. Meng, Y. Xing, C. Wang, F. Li, Y. Wang, X. Wu, Enhanced photocatalytic activity of hierarchically structured BiVO4 oriented along {040} facets with different morphologies, Mater. Lett. 147 (2015) 1–3, https://doi.org/10.1016/j.matlet.2015.02.021.
[44] L. Li, B. Yan, BiVO4/Bi2O3 submicrometer sphere composite: microstructure and photocatalytic activity under visible-light irradiation, J. Alloys. Compd. 476 (2009) 624–628, https://doi.org/10.1016/j.jallcom.2008.09.083.
[45] L.S. Kumari, P.P. Rao, A.N.P. Radhakrishnan, V. James, S. Sameera, P. Koshy, Brilliant yellow color and enhanced NIR reflectance of monoclinic BiVO4 through distortion in VO43- tetrahedra, Sol. Energy Mater. Sol. Cells 112 (2013) 134–143, https://doi.org/10.1016/j.solmat.2013.01.022.
[46] M. Wu, Q.F. Jing, X.Y. Feng, L.M. Chen, BiVO4 microstructures with various morphologies: synthesis and characterization, Appl. Surf. Sci. 427 (2018) 525–532, https://doi.org/10.1016/j.apsusc.2017.07.299.
[47] V.I. Merupo, S. Velumani, G. Oza, M. Makowska-Janusik, A. Kassiba, Structural, electronic and optical features of molybdenum-doped bismuth vanadium oxide, Mat Sci Semicon Proc 31 (2015) 618–623, https://doi.org/10.1016/j.mssp.2014.12.057.
[48] Q. Shi, W. Zhao, L. Xie, J. Chen, M. Zhang, Y. Li, Enhanced visible-light driven photocatalytic mineralization of indoor toluene via a BiVO4/reduced graphene oxide/Bi2O3 all-solid-state Z-scheme system, J. Alloys. Compd. 662 (2016) 108–117, https://doi.org/10.1016/j.jallcom.2015.12.032.
[49] C. Díaz-Guerra, P. Almodóvar, M. Camacho-López, S. Camacho-López, J. Piqueras, Formation of β-Bi2O3 and δ-Bi2O3 during laser irradiation of Bi films studied in-situ by spatially resolved Raman spectroscopy, J. Alloys. Compd. 723 (2017) 520–526, https://doi.org/10.1016/j.jallcom.2017.06.263.
[50] L. Zhang, D. Chen, X. Jiao, Monoclinic structured $BiVO_4$ nanosheets: hydrothermal preparation, formation mechanism, and coloristic and photocatalytic properties, J. Phys. Chem. B 110 (2006) 2668–2673, https://doi.org/10.1021/jp056367d.
[51] A. Walsh, Y. Yan, M.N. Huda, M.M. Al-Jassim, S.H. Wei, Band edge electronic structure of BiVO4: elucidating the role of the Bi s and V d orbitals, Chem. Mater. 21 (2009) 547–551, https://doi.org/10.1021/cm802894z.
[52] S.D. Abraham, S.T. David, R.B. Bennie, C. Joel, D.S. Kumar, Eco-friendly and green synthesis of BiVO4 nanoparticle using microwave irradiation as photocatalayst for the degradation of Alizarin Red S, J. Mol. Struct. 1113 (2016) 174–181, https://doi.org/10.1016/j.molstruc.2016.01.053.
[53] W.A. Thompson, C. Perier, M.M. Maroto-Valer, Systematic study of sol-gel parameters on TiO2 coating for CO2 photoreduction, Appl. Catal. B 238 (2018) 136–146, https://doi.org/10.1016/j.apcatb.2018.07.018.
[54] M.R. Hasan, S.B. Abd Hamid, W.J. Basirun, Charge transfer behavior of graphene-titania photoanode in CO2 photoelectrocatalysis process, Appl. Surf. Sci. 339 (2015) 22–27, https://doi.org/10.1016/j.apsusc.2015.02.162.
[55] M. Jitaru, Electrochemical carbon dioxide reduction - fundamental and Applied Topics (REVIEW), J. Univ. Chem. Technol. Metall. 42 (2007) 333–344.
[56] M. Subrahmanyam, S. Kaneco, N. Alonso-Vante, A screening for the photo reduction of carbon dioxide supported on metal oxide catalysts for C1–C3 selectivity, Appl. Catal. B 23 (1999) 169–174, https://doi.org/10.1016/S0926-3373(99)00079-X.
[57] D. Shi, Y. Feng, S. Zhong, Photocatalytic conversion of CH4 and CO2 to oxygenated compounds over Cu/CdS–TiO2/SiO2 catalyst, Catal. Today 98 (2004) 505–509, https://doi.org/10.1016/j.cattod.2004.09.004.
[58] J.F. de Brito, A.R. Araujo, K. Rajeshwar, M.V.B. Zanoni, Photoelectrochemical reduction of CO2 on Cu/Cu2O films: product distribution and pH effects, Chem. Eng. J. 264 (2015) 302–309, https://doi.org/10.1016/j.cej.2014.11.081.
[59] K.P. Kuhl, E.R. Cave, D.N. Abram, T.F. Jaramillo, New insights into the electrochemical reduction of carbon dioxide on metallic copper surfaces, Energy Environ. Sci. 5 (2012) 7050–7059, https://doi.org/10.1039/C2EE21234J.
[60] J. Jiang, X. Zhang, P. Sun, L. Zhang, ZnO/BiOI heterostructures: photoinduced charge-transfer property and enhanced visible-light photocatalytic activity, J. Phys. Chem. C 115 (2011) 20555–20564, https://doi.org/10.1021/jp205925z.
[61] J.F. Brito, F.F. Hudari, M.V.B. Zanoni, Photoelectrocatalytic performance of nanostructured p-n junction NtTiO2/NsCuO electrode in the selective conversion of CO2 to methanol at low bias potentials, J. Co2 Util. 24 (2018) 81–88, https://doi.org/10.1016/j.jcou.2017.12.008.
[62] A. Navaee, A. Salimi, Sulfur doped-copper oxide nanoclusters synthesized through a facile electroplating process assisted by thiourea for selective photoelectrocatalytic reduction of CO2, J. Colloid Interface Sci. 505 (2017) 241–252, https://doi.org/10.1016/j.jcis.2017.05.103.
[63] P. Wang, S. Wang, H. Wang, Z. Wu, L. Wang, Recent progress on photo-electrocatalytic reduction of carbon dioxide, Part. Part. Syst. Charact. 35 (2018) 1700371, , https://doi.org/10.1002/ppsc.201700371.